Friess, F.; Wischke, C.; Lendlein, A.:
Microscopic analysis of shape-shiftable oligo(ε-caprolactone) - based particles.
In: MRS Advances . Vol. 4 (2019) 59 - 60, 3199 - 3206.
First published online by Cambridge University Press: 18.10.2019

DOI: 10.1557/adv.2019.392
https://dx.doi.org/10.1557/adv.2019.392

Microscopic analysis of shape-shiftable oligo(*ε*-caprolactone) - based particles

Fabian Friess[1,2], Christian Wischke[1], Andreas Lendlein[1,2,*]

[1]*Institute of Biomaterial Science and Berlin-Brandenburg Center for Regenerative Therapies, Helmholtz-Zentrum Geesthacht, Kantstr. 55, 14513 Teltow, Germany*
[2]*Institute of Chemistry, University of Potsdam, Germany*
**Correspondence: andreas.lendlein@hzg.de*

ABSTRACT

Spherical particles are routinely monitored and described by hydrodynamic diameters determined, e.g., by light scattering techniques. Non-spherical particles such as prolate ellipsoids require alternative techniques to characterize particle size as well as particle shape. In this study, oligo(ε-caprolactone) (oCL) based micronetwork (MN) particles with a shape-shifting function based on their shape-memory capability were programmed from spherical to prolate ellipsoidal shape aided by incorporation and stretching in a water-soluble phantom matrix. By applying light microscopy with automated contour detection and aspect ratio analysis, differences in characteristic aspect ratio distributions of non-crosslinked microparticles (MPs) and crosslinked MNs were detected when the degrees of phantom elongation (30-290%) are increased. The thermally induced shape recovery of programmed MNs starts in the body rather than from the tips of ellipsoids, which may be explained based on local differences in micronetwork deformation. By this approach, fascinating intermediate particle shapes with round bodies and two opposite sharp tips can be obtained, which could be of interest, e.g., in valves or other technical devices, in which the tips allow to temporarily encage the switchable particle in the desired position.

Introduction

Polymer particles with a polymeric network structure can be programmed in order to exhibit a shape-memory capability [1, 2]. Micronetworks (MNs) of this type can be established by covalent crosslinking of reactive precursors inside the individual particles or droplets [3]. The on-demand shape shift is driven by an entropy elastic recovery of a stored deformation, which is temporarily fixed through solidification of switching domains, e.g., by crystallization [4].

Along with the ability of such particles to show a shape-memory, i.e., to adapt different (non-spherical) shapes, a need for suitable techniques to characterize the particle's size and shape arises [5]. Ideal techniques should be able to process data not only of single particles but particle populations. Other than spherical particles, whose sizes are routinely monitored and described by hydrodynamic diameters determined, e.g., by light scattering techniques [6] [7],

non-spherical particles require techniques capable to determine characteristic dimensional features resulting from the programming process. Herein, the aspect ratio (*AR*), as defined by the ratio of longest and smallest particle axis, can be applied to describe the shape of prolate ellipsoidal particles, which are a result from a programming of spheres by unidirectional stretching.

In this study, light microscopy with automated shape detection was applied for the evaluation of anisotropic (ellipsoidal) SMP particle populations obtained by different programming schemes. These SMP particles were prepared from oligo(*ε*-caprolactone)-precursors and crosslinked to elastic MN particles with shape–memory function. Furthermore, non-crosslinked thermoplastically deformable microparticles (MP) were included to elucidate the effect of network structure on particle deformation. Finally, the thermally induced shape-recovery is monitored microscopically to explore the dependence of shape-recovery characteristics from the *AR* of programmed MN particles.

Experimental

Synthesis of micronetworks

oCL-IEMA with a degree of endgroup functionalization of 99% was synthesized by a nucleophilic addition reaction using linear oCL-diol (8 kDa, Perstorp) and 2-isocyanatoethylmethacrylate (IEMA) as starting materials. Precursor particles were prepared by microfluidic dispersion of oCL-IEMA solutions (4.5 wt.% in ethyl acetate/dichloromethane 1:1 v/v) in aqueous polyvinyl alcohol (PVA; 2.5 wt.%; Mowiol 4-88, Kuraray) and solvent evaporation. MN were obtained by photocrosslinking oCL-IEMA of molten precursor particles in aqueous suspension flowing in a squared quartz glass capillary (308 nm, Excimer, Heraeus; 4.9 min, 92 $mW \cdot cm^{-2}$) [8].

Analysis of material properties

Standard techniques for polymer network characterization were applied, which were adapted to allow a proper evaluation of MNs in some cases and as reported before [3]. Briefly, thermal properties were determined by DSC (DSC 204 F1, Netzsch; second heating run in nitrogen atmosphere, -100 to 150 °C, 10 $K \cdot min^{-1}$) and crystalline morphology by WAXS (D8 Discover X-ray diffractometer, Bruker). Sizes and size distributions of spherical particles (MP, MN) were determined in water by laser diffraction and given as the main peak of the volume-weighted size distribution (Mastersizer 2000 with Hydro 2000 µP-sample unit, Multiple Narrow Mode; Malvern). Beyond that, laser diffraction was conducted in dichloromethane to evaluate the swelling properties of MNs.

Particle deformation, shape analysis and shape switching

MNs were embedded in PVA phantoms (Mowiol 3-85) by casting a MN suspension in a mold as reported before with subsequent deformation in a tensile tester (70 °C; ZP 20, Zwick) to various ε_{ph}. The MN shape was analyzed in aqueous suspension between glass plates with an automated light microscope (Morphology G3, Malvern) and plotted as *AR* distribution based on data of 180-1300 single particles per population, where fractions with a width of 0.25 in the *AR*-value represent single data points as percentage frequencies. These data

points were subsequently fitted by the Gaussian area fit function of Origin software. The aspect ratio *AR* was determined by the ratio of a particles long axis (*x*) and short axes (*y* = *z*):$AR = x \cdot y^{-1}$. Based on a recently reported uniaxial deformation model of spheres [8], a theoretically expected aspect ratio $AR_{th} = f \cdot f^{0.5}$ was calculated by applying a spatial stretching factor in one direction ($f = \varepsilon_{ph} \cdot (100\%)^{-1} + 1$) and by considering a contraction of particles in the other two spatial directions ($f^{-0.5}$). The deviation of the experimentally determined *AR* was expressed as $\Delta AR = AR \cdot AR_{th}^{-1}$). Scanning electron microscopy (SEM) was conducted with Ir-coated samples at a Gemini Supra™ 40 VP (Carl Zeiss NTS, Oberkochen, Germany), with particle size determination by ImageJ software. The shape switching was studied on a heating stage with microscopic examination (Axio Imager.A1m, Zeiss, 10 $K \cdot min^{-1}$) as reported before [3].

Results and discussion

Synthesis of MN particles and programming to different shapes

In order to synthesize the MNs, linear oligo(*ε*-caprolactone)diol [oCL; 8 kDa] was first functionalized with 2-isocyanatoethylmethacrylate (IEMA) leading to photocrosslinkable precursors. Organic oCL-IEMA solutions were templated into droplets by oil-in water emulsification in a microfluidic setup with subsequent solvent evaporation, resulting in spherical precursor microparticles (MP) of very narrow size distribution (Fig. 1A). By static light scattering, volume-moment mean hydrodynamic particle sizes of MPs dispersed in water were determined to be d_{MP} = 12.5 µm (Uniformity = 0.02), which was confirmed by number-weighted mean diameters of 11.76 ± 0.28 µm as determined from SEM images. In order to prepare MNs with a crosslinked polymer network structure in each individual particle, MPs were dispersed in an aqueous phase, molten and exposed to UV irradiation (308 nm) to induce radical polymerization of the methacrylate moieties [8]. The size and size distribution of spherical MNs obtained by this process did not show alterations compared to the original MP precursors (Fig. 1A).

The existence of a network structure in MNs was confirmed by swelling studies in dichloromethane, where a degree of swelling *Q* of 350 ± 5 vol.% was determined. According to Flory-Rehner theory, a segment length between netpoints M_c of 520 ± 20 Da can be estimated. Comparing the molecular weight of the precursors of 8 kDa, this suggests a relevant contribution of physically netpoints to the network properties in addition to covalent netpoints, which are formed by the reaction of IEMA to oligoacrylates.

For the transfer of particles into a non-spherical prolate ellipsoidal shape, a stretching method was employed, which is based on the application of water soluble PVA. The particles were embedded in PVA films (phantoms), which were subjected to different degrees (30-290%) of phantom elongation $\varepsilon_{ph} = [(l_{prog} / l_0) - 1] \cdot 100\%$ as illustrated in Fig. 1B. The programming step was conducted at 70 °C, which is above the melting temperature $T_{m,MN}$ = 45.2 ± 0.2 °C, i.e. the switching domains formed by oCL chains are in a molten state. This was followed by cooling below T_m to fix the anisotropic shape of the particles by oCL crystallization. The deformed portions of the stretched phantoms were collected and ellipsoidal MPs or MNs were harvested (Fig. 1C) by PVA dissolution. The codes of programmed samples state the applied ε_{ph}, e.g. MN (175).

Distinct conceptual differences apply for MNs and MPs during this deformation process. While oCL-based switching segments integrated in the polymer network structure of MNs should be entropy-elastically deformed, MPs undergo thermoplastic flow above their T_m as they do not possess a covalent network architecture. Interestingly, SEM images of MNs revealed sharper tips after elastic deformation compared to MPs, which will be discussed below. While some defects were observed in MPs after stretching deformation, programmed MNs showed an intact body apparently stabilized by the network architecture.

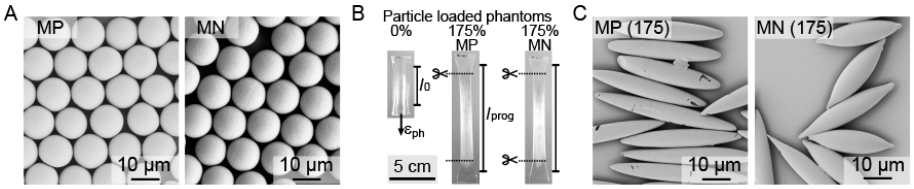

Fig. 1: Preparation of anisotropic particles from spherical templates. (A) SEM images of microparticles (MPs) and micronetworks (MNs) prepared thereof by internal crosslinking of polymer chains. (B) Programming by embedding and stretching in PVA phantoms at ε_{ph} of 30-290%, here exemplarily at 175%. (C) SEM images of particles as isolated from the phantoms after stretching by 175%.

Automated light microscopy to study particle shape distributions

As a core part of this study, automated light microscopy for characterizing populations of non-spherical MPs and MNs should be evaluated. This technique should allow the rapid optical analysis of particle characteristics, such as size and shape, for a relatively large number of particles. In contrast to techniques like SEM, which is often associated with sample modification by sputtering and other conditions potentially creating artefacts, automated light microscopy allows a scanning in native state. Furthermore and as applied here, by imaging and evaluating aqueous particle suspensions, the presences of water meets the typical conditions of application. Each object detected by a contrast difference compared to the background is shape-analysed by a fitting of its contour. Since there is a minimum mobility of micrometer-sized particles in this setup and ellipsoids orientate with their long axis in a horizontal position, the maximum projection areas of the respective particles becomes visible. To obtain accurate and representative data, the raw data are processed after acquisition with filter parameters to exclude inaccurate images, e.g. images of particles with insufficient contrast. In comparison, light scattering techniques like laser diffraction with a strong mobility of particles in a flow-through-system result in a statistical distribution of particle orientations towards the laser and detector, i.e. apparently broad size distributions even for homogeneously sized particles, while particle shapes are no primary or quantitative result of this technique [9].

In a first step, the microscopic images isolated for individual particles were examined (Fig. 2A). Despite starting from perfectly monodisperse and spherical templates (MN or MP), slight differences in particle shapes were microscopically visible for a given ε_{ph}. Specifically, when the particles of a single data-set were analysed for their mean *AR*, a portion of particles with lowest and highest AR could be identified and displayed (Fig. 2A). This distribution within the particle populations may be explained by a statistical variation of crosslinking density for individual particles or by a slight distribution of local phantom

deformation during stretching, which is highest in the centre of the phantom. Here, particles from the entire deformed phantom portion (except their very ends) were collected to allow for a certain level of shape distribution in order to challenge the automated microscopy technique, while more homogeneous populations might be obtained by isolating particles from the core portion of stretched phantoms only.

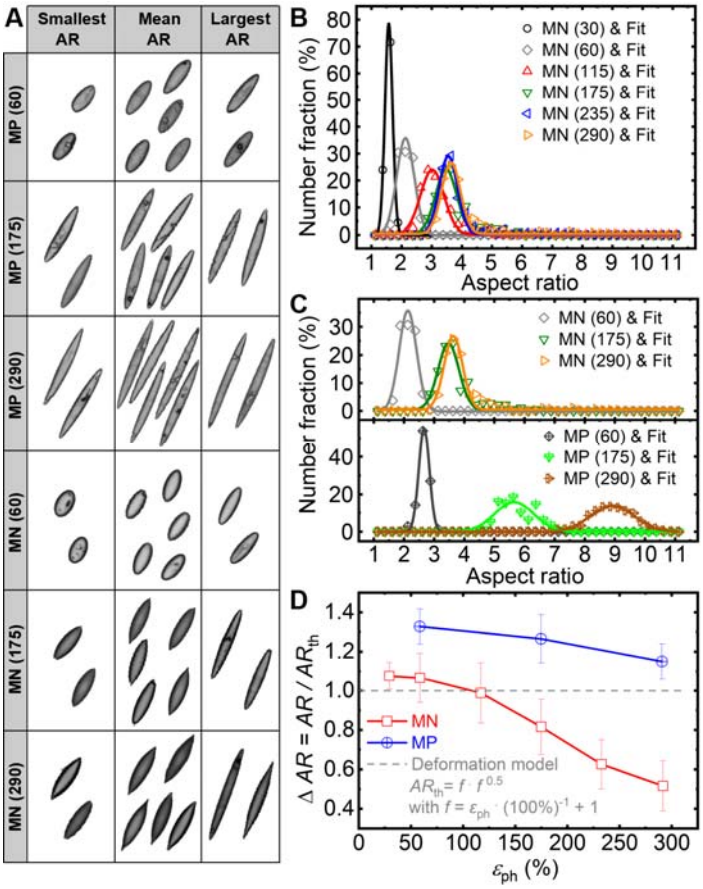

Fig. 2: Analysis of shape distribution of MNs and MPs by automated light microscopy and data analysis. (A) Representative microscopic images of individual particles in different *AR* ranges. (B-C) Effect of ε_{ph} (B) and crosslinking (C) on the *AR* distribution of deformed particles. Experimental data (individual symbols) and Gaussian fit (full line). (D) Analysis of deviation of MP and MN from a deformation model.

In a next step, the effect of ε_{ph} on the MNs shape was studied by the width and peak position of the *AR*-distribution. Automated light microscopy allowed distinguishing substantial shifts in the *AR* of MN upon programming as expected. However, the *AR* increased only to a certain point and did not further increase relevantly when ε_{ph} was 175 to 290% (Fig 2B). At the same time, plotting the *AR* data and applying a Gaussian curve fitting illustrated a minor and

finite increase of the *AR*-distribution width for the main portion of the programmed MNs, according to the concept of local phantom deformations introduced above.

The lack of further MN deformation might originate either from boundaries of deformability of the elastic MN or from a limited stress transfer at the interphases of particles and PVA phantoms. In order to characterize the effect of the polymer network structure of MN on deformability, non-crosslinked MPs were studied in the same way as a control set (Fig. 2C). For MPs, a substantially higher *AR* and larger width of the AR distribution was observed compared to MNs at identical ε_{ph}. Recently, a simplified deformation model was presented to estimate theoretical AR_{th} expected from uniaxially stretching of spheres [8]. When determining the deviation ΔAR of experimental data from this model, MNs matched the model for a certain range of ε_{ph} with a subsequently drop of deformability. For MPs, the elongated shapes had higher ΔAR than MN over the full range of studied ε_{ph} with values above those suggested by the model, presumably due to their very easy deformability in the molten state. Overall, it is plausible to conclude that the internal network structure of MNs restricted the elastic deformation, while MP's thermoplastic deformability leads to higher *ARs*.

Shape recovery characteristics

The mechanical stress temporarily stored in programmed MNs can be released by heating the samples over T_m, where oCL chain segments in the switching domain acquire sufficient mobility for elastic recoil towards a relaxed state. This molecular reorientation forms the basis for the samples' shape-shifting by the shape-memory effect. When MN (115) and MN (290) were microscopically monitored during temperature-induced shape-recovery with continuous heating, the general ability of all MNs to switch shape at ~45 °C matching $T_{m,MN}$ was confirmed without major differences between the samples (Fig. 3).

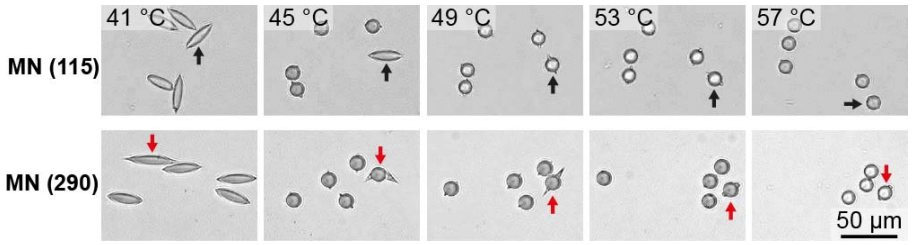

Fig. 3: Shape recovery features of MNs (115) and MNs (290) in a continuous heating experiment with microscopic observation.

An interesting observation concerned the pattern of the shape switching on the single particle level and the intermediate states being adapted. Shape switching did not start from the tips, which have highest surface-to-volume ratio and should encounter the largest forces by interfacial tension, which is oriented in the same direction as the entropy elastic forces for the switching from ellipsoidal to spherical shapes. Instead, switching started from the particles' centre, where the largest volume of MN material is present. At the same time,

remains of the tips were present clearly above $T_{m,MN}$ at temperatures above, e.g., 49 °C, and decreased in size upon further heating. The observation of the sharp tips of the programmed MN in contrast to the less sharp tips of stretched MP (Fig. 1C) and the switching pattern (Fig. 3) might be related to local molecular and morphological differences throughout the individual MN.

A number of principles may either individually or synergistically contribute to the observed shape-shifting pattern: The capability for shape recovery depends on the integrity of the covalent network structure as defined by covalent netpoints and oCL switching segments, which connect these netpoints. Potential network damages at the particle tips as regions of apparently high deformation, i.e. breaking of covalent bonds, would result in a decay of recovery forces. It is also relevant to note that remaining tips were more expressed at those particles of a given particle population, which had larger *AR* initially, supporting an assumption of a lower network density due to less efficient crosslinking and/or stretching-induced network alteration. In case of network damage, interfacial tension may dominate as driving force for shape alteration by a plastic flow, which was previously shown to be slow in non-crosslinked particles until the T_m of the precursor is clearly exceeded [3]. For non-crosslinked oCL starting material, a $T_{m,oCL}$ = 54 °C was determined, which is about the temperature at which the tips slowly disappeared. Another relevant aspect might be the quantity of oCL crystallites, which can block shape recovery, in different particle locations. While WAXS studies allowed determining the overall degree of crystallinity *DOC* of 27.2 ± 3.1% and the crystallite size l_c of 16.4 ± 0.1 nm of MN powders, the local content of crystallites remains unknown. As surfaces may contribute to oCL crystallisation and surface to bulk-material ratios vary in different particle locations, phenomena associated to the mass content of crystallites may be involved.

Advantageously, as the extent of shape-shifting of the tips is systematically linked to the applied temperature, an interrupted heating approach will result in micrometer-sized particles from a single material with unique shapes that may not be easily assessable by other techniques. They could serve for mechanistic evaluation of cellular uptake in curiosity-driven research considering a known effect of the angle of particle contact with cells [10]. In technical fields, they could be evaluated as functional components in the future, e.g., as micro-propellers or as flow sensors, or by employing the tips to temporarily encage the switchable particles in a desired position as relevant for one-time valves.

Conclusions

Automated microscopy enabled the characterization of large sets of shape-shiftable MN particles and their non-crosslinked analogues (MPs) with different prolate ellipsoidal shapes. In this way, relevant differences in the shape distribution of particle populations were distinguished. For example, starting from monodisperse spherical templates, the *AR* and *AR*-distribution as well as the limits of deformation and the shape of ellipsoid's tips are clearly affected by polymer network architecture and programming conditions as could be concluded via the employed methodology. Almost identical populations of particles could be assigned into subpopulations. Furthermore, this study reveals a distinct pattern of shape-recovery behaviour of MN tips at increasing temperatures, which gives access to fascinating intermediate particle shapes with round bodies and sharp tips.

Acknowledgments

We are grateful for program-oriented funding by the Helmholtz-Association. Additionally, we thank Daniela Radzik and Yvonne Pieper for technical support.

References

[1] C. Wischke, M. Schossig, A. Lendlein, Shape-Memory Effect of Micro-/Nanoparticles from Thermoplastic Multiblock Copolymers, Small, 10 (2014) 83-87.
[2] S.M. Brosnan, A.-M.S. Jackson, Y. Wang, V.S. Ashby, Shape Memory Particles Capable of Controlled Geometric and Chemical Asymmetry made from Aliphatic Polyesters, Macromolecular Rapid Communications, 35 (2014) 1653-1660.
[3] F. Friess, U. Nochel, A. Lendlein, C. Wischke, Polymer Micronetworks with Shape-Memory as Future Platform to Explore Shape-Dependent Biological Effects, Adv Healthc Mater, 3 (2014) 1986-1990.
[4] G.I. Peterson, A.V. Dobrynin, M.L. Becker, Biodegradable Shape Memory Polymers in Medicine, Adv Healthc Mater, 6 (2017).
[5] R. Mathaes, G. Winter, J. Engert, A. Besheer, Application of different analytical methods for the characterization of non-spherical micro- and nanoparticles, Int J Pharmaceut, 453 (2013) 620-629.
[6] F. Caputo, J. Clogston, L. Calzolai, M. Rosslein, A. Prina-Mello, Measuring particle size distribution of nanoparticle enabled medicinal products, the joint view of EUNCL and NCI-NCL. A step by step approach combining orthogonal measurements with increasing complexity, J Control Release, 299 (2019) 31-43.
[7] E. Laborda, A. Molina, C. Batchelor-McAuley, R.G. Compton, Individual Detection and Characterization of Non-Electrocatalytic, Redox-Inactive Particles in Solution by using Electrochemistry, Chemelectrochem, 5 (2018) 410-417.
[8] F. Friess, T. Roch, B. Seifert, A. Lendlein, C. Wischke, Phagocytosis of spherical and ellipsoidal micronetwork colloids from crosslinked poly(ε-caprolactone), Int J Pharmaceut, 567 (2019) 118461.
[9] T. Matsuyama, H. Yamamoto, Particle shape and laser diffraction: A discussion of the particle shape problem, J Disper Sci Technol, 25 (2004) 409-416.
[10] J.A. Champion, S. Mitragotri, Role of target geometry in phagocytosis, P Natl Acad Sci USA, 103 (2006) 4930-4934.